Identifying Order and Disorder in Double Fourmembered Rings Via Raman Spectroscopy During Crystallization of LTA Zeolite

Song Luo,^{1#} Tongkun Wang,^{2#} Jason Gulbinski,¹ Long Qi,³ Geoffrey A. Tompsett,⁴ Michael T. Timko,⁴ Scott M. Auerbach,^{1,2*} and Wei Fan^{1*}

¹Department of Chemical Engineering, University of Massachusetts Amherst, Amherst, Massachusetts 01003, United States

²Department of Chemistry, University of Massachusetts Amherst, Amherst, Massachusetts 01003, United States

³U.S. DOE Ames Laboratory, Iowa State University, Ames, Iowa 50011, United States

⁴Department of Chemical Engineering, Worcester Polytechnic Institute, Worcester, Massachusetts 01609, United States

E-mail: <u>auerbach@umass.edu</u>, <u>wfan@ecs.umass.edu</u>

*S.L. and T.W. contributed equally to this work.

ABSTRACT: Fluoride (F⁻) has been essential for the synthesis of low-defect siliceous zeolites. It has been hypothesized that F balances the positive charges from organic structure-directing agents (OSDA) and stabilizes key building units during zeolite crystallization such as the double fourmembered ring (D4R). However, due to the lack of characterization techniques for investigating medium-range structures, including rings and cages formed during zeolite crystallization, the roles of F in stabilizing building units and maintaining local charge balance during zeolite assembly are not yet fully understood. Here, the crystallization of siliceous LTA zeolite in the presence of F was investigated using Raman spectroscopy and periodic DFT calculations. We have discovered that the F-filled double four-membered ring (F-/D4R) and the empty D4R exhibit rather distinct Raman features. Both F-/D4R and empty D4R are formed in the LTA zeolite synthesized in the presence of F using 1,2-dimethyl-3-(4-methylbenzyl) imidazolium as the OSDA. Observed Raman bands of F-/D4R and empty D4R, along with predictive DFT calculations on LTA supercells, reveal an ordered distribution of these two D4R units in the final as-made LTA zeolite. The discovery of these distinct Raman signatures of F-/D4R and empty D4R units opens an interesting new window for studying defects in D4R during zeolite formation. In particular, we have observed variation in Raman intensities of F-/D4R and empty D4R bands during LTA crystallization; periodic DFT calculations indicate that the observed Raman behavior is consistent with empty D4R units containing one or two Si vacancies surrounded by Q₃ Si – consistent also with solid-state NMR measurement. These defects appear to heal during further crystallization, leading to the formation of defect-free LTA zeolite crystals. Overall, our results provide deeper understanding on the roles of F⁻ in charge balancing and stabilizing intact D4R units during zeolite formation.

INTRODUCTION

Zeolites are crystalline microporous structures with pore sizes ranging from 0.3 nm to 2 nm with important applications in catalysis, separations, and several emerging areas.¹⁻⁴ The great diversity of zeolite structures and compositions arises from an equally great collection of synthetic protocols that have been discovered over the last seven decades through laborious research.⁵⁻⁷ Despite these massive efforts, the atomic-level events involved in zeolite crystallization processes remain largely unknown.⁸⁻¹⁰ Better understanding of these events in zeolite assembly could help unlock a treasure trove of hypothetical zeolite structures,¹¹⁻¹³ many of which show promise for emerging applications such as carbon capture¹⁴ and clean energy production.¹⁵ Herein, the crystallization of LTA zeolite in the presence of F⁻ was investigated using Raman spectroscopy and periodic DFT calculations with the aim of probing the assembly of building units and defect structures formed during the crystallization process.

In general, zeolites can be synthesized in alkaline media at high pH, or in fluoride media under more neutral conditions, with OH⁻ and F⁻ required as mineralizing agents for crystallization.¹⁶⁻¹⁸ The fluoride synthesis route, which was invented by Flanigen and Patton, ¹⁸ has been extensively developed during the last three decades and has led to a variety of new, defect-free microporous materials – essentially high-silica or even all-silica zeolites.^{17, 19} Zeolite chemists have hypothesized that F⁻ creates new zeolite structures via (*i*) a structure-directing effect of F⁻ stabilizing small silicate rings and cages such as the double four-membered ring (D4R) unit in zeolites,²⁰⁻²³ and (*ii*) a charge-compensating role, where F⁻ balances the positive charges from organic structure-directing agents (OSDAs), thus removing the need for negatively-charged framework defects.^{17,24-25} To date, the synthesis of siliceous zeolites containing the D4R is possible only through the F-mediated route,²⁶⁻²⁹ with F⁻ inside the D4R²³ or by a post-synthetic method

called assembly–disassembly–organization–reassembly (ADOR). ³⁰⁻³² After crystallization, the F-inside the D4R cannot be removed by ambient ion-exchange, ^{33,34} suggesting that D4R may form around F- in a kind of directed assembly process. Interestingly, it has also been found that D4R in siliceous zeolites remains stable even after the removal of F- by calcination. ³³⁻³⁴ These intriguing observations prompt the following fundamental questions: How do F-filled D4R units (F-/D4R) form, and how do these units assemble to make zeolites? Can the echoes of this assembly process be discerned by discovering defects and disorder left behind in F-/D4R units? How can such defects and disorder be probed during zeolite formation? Below we make a substantial step in answering these questions by integrating experimental zeolite synthesis and characterization by Raman spectroscopy with periodic DFT calculations.

The structure of zeolite LTA comprises one large cavity (α -cage), three smaller cavities (β -cages), and three connecting D4R units in each LTA unit cell (see Fig. 1). LTA is a fascinating nanoporous network because these building blocks can contain distinct chemical moieties that allow rigorous investigations of the structure-directing hypotheses for the F⁻ mediated synthesis. Furthermore, LTA is one of 38 zeolite topologies featuring the D4R,³⁵ a zeolite building unit that is stabilized by inclusion of F⁻ based on its size and electronic properties, as shown by gas-phase electronic structure calculations.²⁰ Therefore, as a model system, investigating the crystallization of zeolite LTA in the presence of F⁻ provides a unique opportunity to address fundamental questions regarding the role of F⁻ in zeolite formation.

Despite the long history of zeolite synthesis and characterization research, investigating zeolite crystallization processes remains challenging mainly due to the lack of characterization techniques that can examine medium-range structures including rings and cages formed during zeolite assembly.³⁶ Raman spectroscopy has emerged as a critical tool for probing medium-range

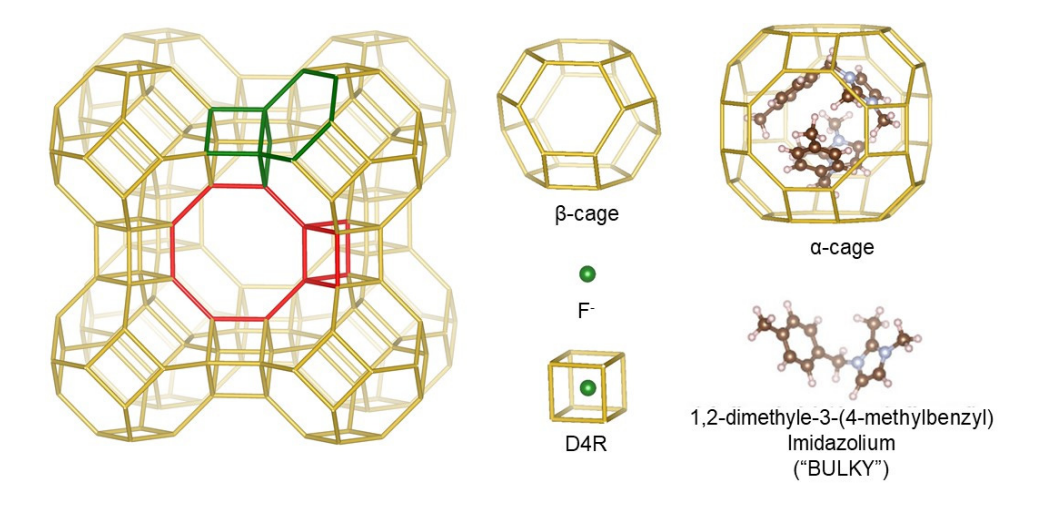


Figure 1. LTA zeolite structure and its three building subunits: one α -cage, one β -cage, and three double four-membered rings (D4R) per unit cell. Each subunit may contain species as shown in the figure. Synthesis with a dimer of BULKY cations would require 2/3 of D4R to be filled with F⁻ according to charge-balancing hypothesis. 4-4-6 and 4-4-8 tricyclic bridges in siliceous LTA are highlighted in green and red, respectively.

structures in a range of silica network assemblies,³⁷⁻⁴¹ complementing shorter-range techniques such as NMR and longer-range information from X-ray diffraction (XRD).⁴²⁻⁴³ However, assignments of Raman bands to specific rings and cages have largely been made by inductive reasoning that must be confirmed by predictive calculations.

We have addressed the issue of Raman band assignments in our recent work through a systematic synthesis, spectroscopy, and periodic DFT study of several siliceous zeolites with various frameworks.³⁹ Normal mode analysis suggests that Raman bands should be assigned to tricyclic bridges – three zeolite rings that share a common Si-O-Si bridge, rather than to individual rings. For example, while Raman bands at ~500 cm⁻¹ for zeolites have typically been assigned to 4-membered ring vibrations,⁴⁴ normal mode analysis applied to siliceous LTA indicates that the Raman band at 506 cm⁻¹ results from vibrations of 4-4-6 and 4-4-8 tricyclic bridges (green and red, respectively, in Fig. 1), where "*x-y-z*" denotes a tricyclic bridge connecting an *x*-ring, a *y*-ring, and a *z*-ring. These 4-4-6 and 4-4-8 tricyclic bridges in LTA come together to comprise the D4R, indicating that the LTA Raman band at 506 cm⁻¹ corresponds to symmetric breathing of the D4R.

We have also discovered, via the concept of tricyclic bridges, a strong anti-correlation between Raman frequency and Si-O-Si angle. Rigorous assignment of Raman bands arising from specific zeolite structures provides new avenues for studying the role of structural defects in zeolite crystallization.

Here we apply zeolite synthesis, Raman spectroscopy, and periodic DFT to investigate the effects of F⁻ on the structures of subunits formed during the crystallization of siliceous LTA zeolite. Our discovery of distinct Raman signatures of F⁻-filled and empty D4R units has revealed detailed information on the evolution of these units during the crystallization process. Such insights are fundamentally important for understanding the hierarchical nature of zeolite crystallization mechanisms and may also assist in designing syntheses of zeolites with new structures and compositions.

RESULTS AND DISCUSSION

Here we detail and discuss our results on the F-mediated synthesis of LTA using BULKY as the OSDA; the Raman spectroscopy of as-made LTA-BULKY-F distinguishing empty D4R and F-/D4R units; using Raman to study the crystallization process of LTA; and applying the insights gained to create a scalable synthesis of Si-LTA with substantially reduced HF.

Synthesis of LTA-BULKY-F: Synthesis of siliceous LTA zeolite in the presence of F-was pioneered by Corma *et al.* using dimers of bulky OSDA cations.²⁹ This method was extended by Davis *et al.*⁴⁵ who synthesized LTA using dimers of 1,2-dimethyl-3-(4-methylbenzyl) imidazolium (herein denoted as "BULKY"), which occupies the α -cage in a structural motif akin to two hands packing a snowball (Fig. 1). Because the α -cage is occupied by two BULKY molecules and the β -cage is empty, only two out of three D4Rs per unit cell are theoretically

occupied with F⁻ to achieve charge balance in the zeolite. As a result, we expect to find the presence of both F⁻/D4R and empty D4R in the LTA synthesized using BULKY, possibly with distinct Raman signatures.

LTA-BULKY-F was synthesized using a gel composition of 1.00 SiO₂: 0.50 HF: 0.50 BULKY-OH: 5.00 H₂O with addition of 7 wt.% LTA seeds with regard to silica source, following the literature method. ⁴⁵ Aluminosilicate LTA nanocrystals (Si/Al=1.26) with a size of around 200 nm were used as seeds for the crystallization. Highly crystalline LTA crystals were obtained after hydrothermal synthesis at 170 °C for 8 days. The synthesized LTA exhibits a Si/Al ratio of 66. Strictly speaking the LTA sample is not a siliceous zeolite. However, the aluminum content is approximately one aluminum atom per three unit cells, indicating that the LTA zeolite is close to but not precisely a siliceous zeolite. To determine the effects of Al on the Raman spectra we conducted a periodic DFT study, finding insignificant effects on computed Raman spectra from these very low Al contents, as shown in the SI (Figs. S14 (a) and (b)). The effect of Al on the charge balancing is discussed in detail below.

Raman Signatures of F-/D4R and Empty D4R: Fig. 2a shows experimental and DFT-computed Raman spectra of LTA synthesized using BULKY as the OSDA, including spectra obtained both before and after calcination. The Raman spectrum obtained from the sample after calcination (experiment: green; DFT: red) reveals a prominent band around 500 cm⁻¹ (shaded yellow) assigned by DFT to the combination of 4-4-6 and 4-4-8 tricyclic bridge vibrations, which as discussed in the Introduction, come together to comprise the empty D4R symmetric breathing mode. Fig. 2a shows that periodic DFT using the PBE functional accurately reproduces this experimental Raman spectrum, with a consistent red shift of about ~20 cm⁻¹ characteristic of PBE (frequencies are left unscaled).

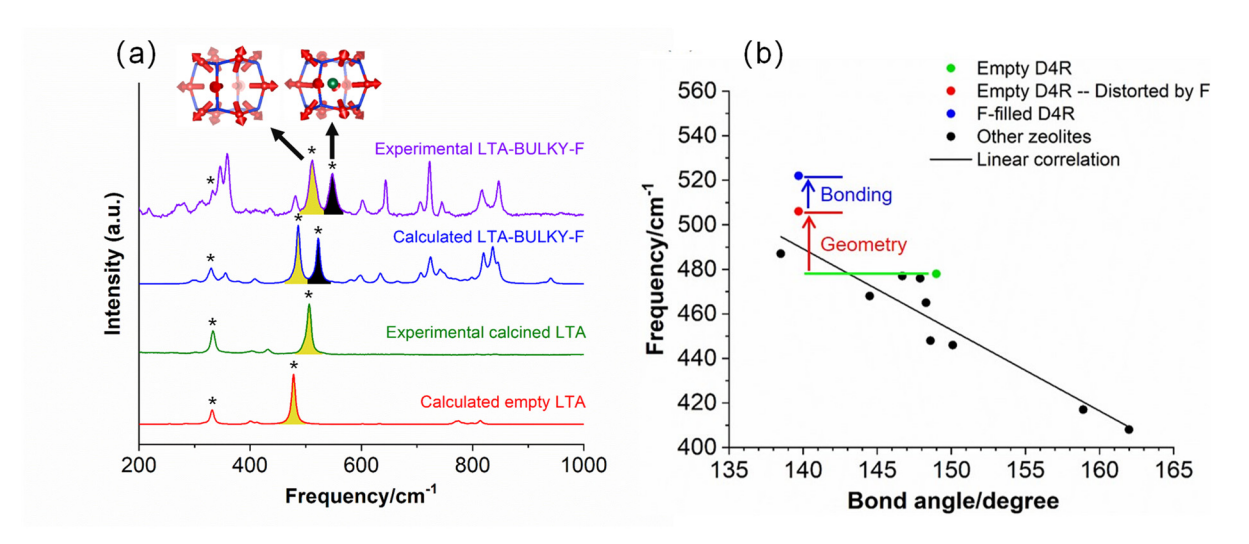


Figure 2. (a) Raman spectra of calcined LTA (experiment in green, DFT in red) and as-made LTA before calcination (experiment in purple, DFT in blue) showing excellent agreement between experiment and theory, with DFT exhibiting red-shifts from measured band locations. Raman bands for LTA vibrations are marked with black star; unmarked bands are assigned by DFT to BULKY OSDA; yellow-shaded band is empty D4R symmetric breathing mode; black-shaded band is assigned by DFT to F-filled D4R (F-/D4R). **(b)** Periodic DFT analysis of blue-shift of D4R Raman band from empty (green dot) to F-filled (blue dot): most of blue-shift explained by geometrical distortion of D4R (decrease in Si-O-Si angle, red dot); remaining blue-shift attributed to unique F-/D4R bonding interaction.

Periodic DFT was further used to simulate the Raman spectrum of LTA-BULKY-F before calcination, with two molecules of BULKY in the α-cage and two F⁻ ions in the D4R. As shown in Fig. 2a, comparing the experimental (purple) and simulated spectra (blue) shows that periodic DFT using the PBE functional also reproduces most features of the Raman spectrum of as-made LTA. Normal mode analysis allows us to distinguish the Raman bands from the BULKY OSDA and zeolite lattice, respectively, which is critical for utilizing Raman spectroscopy to investigate zeolite samples synthesized in the presence of OSDA. Raman bands in Fig. 2a marked with a black star correspond to the vibrations of LTA lattice, whereas the unmarked bands in Fig. 2a are assigned to the vibrations of the BULKY OSDA – consistent with Raman spectra of BULKY in salt and aqueous phases (see Fig. S1). Interestingly, two Raman bands associated with the D4R in LTA-BULKY-F sample before calcination were observed in Fig. 2a. These Raman bands are

shaded in yellow and black and are assigned by DFT to D4R symmetric breathing modes (combining 4-4-6 and 4-4-8 tricyclic bridges) of empty D4R (yellow) and F⁻/D4R (black). This assignment, relying on normal mode analysis, is in agreement with the previous Raman assignment (based on comparative and inductive reasoning) for AST zeolite, in which the 491 cm⁻¹ and 524 cm⁻¹ bands were assigned to empty and F-filled D4R units of AST, respectively.^[47] The DFT-predicted bands appear at 490 cm⁻¹ (empty D4R) and 524 cm⁻¹ (F⁻/D4R) – a predicted band separation of 34 cm⁻¹; while the measured Raman bands appear at 512 cm⁻¹ and 548 cm⁻¹ (observed separation of 36 cm⁻¹), indicating quantitative agreement on this band separation. The presence of empty D4R in LTA-BULKY-F is intriguing since previous studies³⁰⁻³² have suggested that siliceous D4R units in zeolites can only be formed in the presence of F⁻ (unless using the post-synthetic ADOR method).

Structure and Dynamics of F⁻/D4R via Raman: To better understand how the interaction between F⁻ and the D4R influences the Raman signature of the F⁻/D4R unit, we investigated the frequencies of the empty D4R and F⁻/D4R bands in Fig. 2a to reveal the interplay among geometry, vibrational dynamics, and electronic structure of the F⁻/D4R building unit. Figure 2b displays a periodic-DFT analysis of Raman frequencies associated with F⁻ occupying the D4R. Our previous Raman study reported an anti-correlation between Raman frequency and Si-O-Si angle for several zeolites containing 4-*x-y* tricyclic bridges (black dots in Fig. 2b),³⁹ suggesting we should expect decreased Si-O-Si angles in the D4R upon including F⁻ based on the observed blue shift. Indeed, our periodic DFT calculations indicate a decrease in D4R angles from 146.9° to 139.6° upon including F⁻ (see Table S1), consistent with the expected anti-correlation and previous studies^{20, 48} – but insufficient to explain the full magnitude (34 cm⁻¹) of the calculated blue shift.

Fig. 2b shows DFT-computed Raman band frequencies of the empty D4R (green dot), the F'/D4R (blue dot), and the D4R distorted to the F-filled geometry but still empty (red dot). Including the red point in Fig. 2b provides a way to determine if geometrical distortion alone is sufficient to explain the magnitude of the blue shift. Fig. 2b shows that most of the Raman blue shift ("Geometry" in Fig. 2b) can be explained by the geometrical distortion. However, a significant portion of the blue shift ("Bonding" in Fig. 2b) cannot be explained by D4R distortion alone, indicating a change in Si-O bonding in F-/D4R. This result is consistent with previous calculations finding a unique chemical interaction between F- and D4R involving donation of electron density from F- to frontier orbitals of D4R.^{20, 48} Thus, the Raman blue shift in Fig. 2a and 2b serves as an indicator of both geometrical distortion and charge transfer to D4R upon inclusion of F-.

Ordered and Disordered Fluoride Distributions in LTA. Since not all the D4R units in LTA-BULKY-F are filled with F⁻, both homogeneous and heterogeneous F⁻ distributions are possible. In both cases, we assume two BULKY cations in each α-cage, which is consistent with Elemental Analysis and TGA data (*vide infra*). In the homogeneous case, each unit cell would contain two F⁻/D4Rs and one empty D4R, with the two negative F⁻ charges balancing the two BULKY positive charges. In contrast, a heterogeneous distribution is possible, e.g., where one unit cell contains three F⁻ ions and an adjacent cell contains only one ion. Here we investigate these cases by studying their predicted Raman intensities and band shapes for F⁻/D4R and empty D4R, in comparison with experiments.

We simulated the homogeneous case with a periodic cell comprised of a single LTA unit cell, which produces the calculated Raman spectrum shown in Fig. 2a (blue). The ratio of Raman intensities of F-/D4R and empty D4R bands (denoted I_F/I_E) can shed light on F- distributions. The

experimental data in Fig. 2a give an I_F/I_E value of 0.75, while DFT in the homogeneous case predicts 0.79 – excellent agreement that lends credence to the homogeneous model. Reflecting now on the origin of this intensity ratio, the fact that two D4Rs are F-filled while one is empty would seem to suggest an I_F/I_E value closer to 2. However, we find that both experiment and the homogeneous model find I_F/I_E values closer to unity. The apparent contradiction can be explained by vibrational symmetries in the homogeneous case. In particular, the breathing vibrations of the two F-/D4Rs couple to make symmetric and anti-symmetric normal modes (see Fig. S3), but only the symmetric combination of the two F-/D4R breathing motions exhibits significant Raman intensity. As such, the DFT-computed ratio I_F/I_E is near unity because it compares Raman intensity from one mode of coupled F-/D4Rs to one mode of the empty D4R. Therefore, the excellent agreement between experiment and DFT theory in the homogeneous case – as explained by the coupling of oscillators at high symmetry – seems to argue for a homogeneous fluoride distribution in the LTA-BULKY-F sample.

To test the homogeneous model, we considered the heterogeneous case using a supercell containing two LTA unit cells: one unit cell with two BULKY cations and three F⁻ anions, and the other unit cell with two BULKY and one F⁻. After optimizing coordinates and lattice parameters, the energy of the heterogeneous model was found to be 1.2 eV = 116 kJ/mol greater than the energy of two homogeneous unit cells because of the charge separation between the heterogeneous unit cells. Normalizing this energy difference by the 48 SiO₂ units of the two LTA unit cells gives 2.4 kJ/mol-Si – a value well within the normal range of zeolite framework energies, ⁴⁹ suggesting that the heterogeneous distribution is thermodynamically feasible.

The results of the Raman calculations for the heterogeneous case are shown in Fig. S4 along with the homogeneous result and the experimental Raman spectrum for as-made LTA-

BULKY-F. Careful analyses of the Raman spectra in Fig. S4 reveal two discrepancies between the heterogeneous model and experimental data. First, the F-/D4R to empty D4R Raman intensity ratio (*I_F/I_E*) calculated from the heterogeneous spectrum is 0.61, which is 19% less than the experimental value of 0.75, while the homogeneous prediction (0.79) is within 5.3% of experiment. Second, the heterogeneous model Raman spectrum in Fig. S4 shows a small shoulder band associated with slightly different vibrational frequencies of F-/D4R in the unit cells containing one F- and three F- ions. In contrast, peak fitting of the experimental Raman spectra (Fig. S11) shows no discernable shoulder band for the 8-day sample. Thus, we conclude from these experimental and simulated Raman spectra that fluoride is homogeneously distributed among D4R in the as-made LTA-BULKY-F system.

Overall, the Raman bands for empty D4R and F⁻/D4R in LTA zeolite are found to be rich with information about F⁻/D4R structure, bonding, and spatial distribution, opening the door to investigate defects in crystallization as we show below.

Quantifying Empty D4R and F⁻/D4R in LTA. The F⁻ distribution and the amount of empty D4R and F⁻/D4R in LTA-BULKY-F samples were studied by TGA, elemental analysis, and ¹⁹F/²⁹Si magic angle spinning solid-state NMR (MAS SS-NMR) to shed light on the nature of charge-balancing in the as-made zeolite.

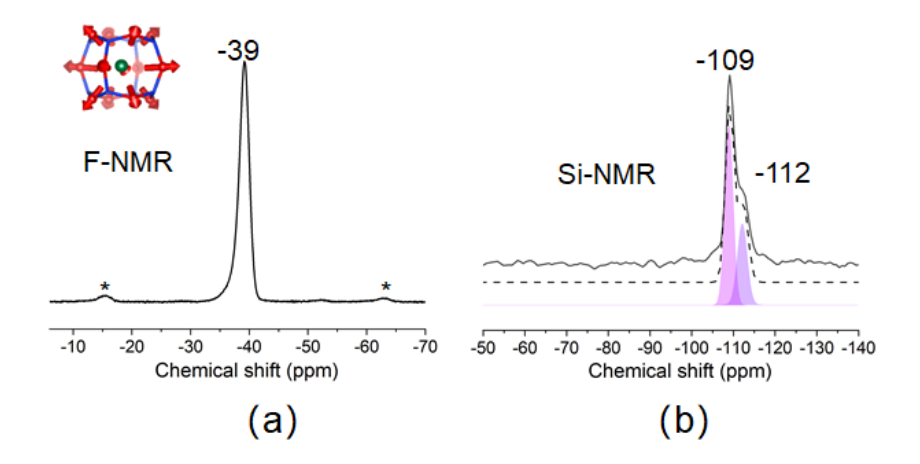


Figure 3. (a) ¹⁹F MAS NMR and **(b)** ²⁹Si MAS solid state NMR spectra of LTA-BULKY-F with peak deconvolution. The peaks marked with asterisk in ¹⁹F MAS NMR spectrum are side bands from the peak at -39 ppm. Two peaks at -109 and -112 ppm in ²⁹Si MAS NMR spectrum are from Si (Q_4) in F-/D4R and empty D4R, respectively.

¹⁹F NMR spectrum as displayed in Fig. 3a and Fig. S7a, consist of a single peak located at -39 ppm, indicating that F^- exclusively resides in the D4R of as-made LTA-BULKY-F samples. This finding is consistent with previous studies and our DFT calculations of ¹⁹F chemical shifts (Table S3), indicating a preferred distribution of F^- in D4R of LTA.^{23, 34, 45} The small anisotropy observed in the ¹⁹F NMR might be due to the non-uniform particle size and shape achieved in the synthesis as shown in Figure S9D. Elemental analysis indicates that the amount of F^- in LTA-BULKY-F is 1.84 ± 0.04 wt.%, which corresponds to 61 ± 2% of D4R filled with F^- (Table S4). TGA weight loss of LTA-BULKY-F is 23.9% (Fig. S5), within 2% of the theoretical loss of 23.4% corresponding to two BULKY and two F^- per unit cell of LTA, suggesting that two BULKY cations reside in each α-cage of LTA-BULKY-F and that the β-cage is empty.⁴⁵

The ²⁹Si NMR spectrum in Fig. 3b shows that there are two peaks located at -109 ppm and -112 ppm for LTA-BULKY-F, indicating that Si atoms in LTA-BULKY-F exhibit two different

local environments. Following Shayib et al.²³ and consistent with our DFT calculations (Table S3 and Fig. S6),²³ the -112 ppm peak is assigned to Si (Q₄) in the empty D4R, and the -109 ppm peak is assigned to Si (Q₄) in the F⁻/D4R. The difference in chemical shift of empty D4R and F⁻/D4R is consistent with results from Shayib et al.²³ on F-/D4R containing ITW zeolite.²³ Because the LTA sample is not strictly a siliceous zeolite but contains small amounts of Al with a Si/Al ratio of 66 determined by elemental analysis, the sample contains some number of Si-O-Al linkages. Due to the negative charge caused by the incorporation of Al into D4R, the Al is more likely distributed in the empty D4R to avoid strong electrostatic repulsion with the F in F-/D4R. Our DFT calculation (Table S3 and Fig. S6) and previous literature⁵⁰ both suggest that incorporating Al into zeolite frameworks causes a peak shift to less negative chemical shifts of around 5 ppm, meaning the NMR peak for Si connected to one Al, Q4(1Al), in empty D4R will overlap the peak form Si atom in F/D4R. As a result, we expect the actual ratio of F/D4R to empty D4R to be less than the ratio obtained from the integrated Si NMR peak area at -109 ppm and -112 ppm. No partially coordinated Si such as Q₃ or Q₂ is observed in LTA-BULKY-F, indicating that the sample is defect-free and that the positive charge from BULKY cations is balanced by negative charge from F ions and the presence of framework Al from seeds. The molar ratio (F+Al)/BULKY, representing the ratio of negative to positive charge, was found by elemental analysis to be 1.05 (Table S4 and analysis below Table S4), indicating a well-understood charge balance in the asmade LTA-BULKY-F sample. This finding lends further credence to the charge-balancing role of F in zeolite synthesis.

Probing Si-LTA Crystallization Using Raman. Raman spectra and XRD patterns were collected at various stages of LTA synthesis using BULKY as the OSDA, to investigate the evolution of empty D4R and F-/D4R units during crystallization. Fig. 4a shows Raman spectra for

samples at the following stages/times of LTA synthesis: the precursor gel (red), 1.5 h (gold), 2.5 h (green), 3 h (teal), 6 h (blue), and 8 day (purple). Fig. 4b shows XRD patterns of the same samples. No diffraction peaks from the LTA seeds were observed in the 1.5 h and 2.5 h samples, and very weak diffraction peaks were observed in the precursor gel. In addition, the same synthesis gel, but without addition of HF, shows the LTA diffraction peaks from the seeds as shown in Fig. S8. Comparison of the XRD patterns of the samples indicates that the LTA seeds were dissolved before the formation LTA crystals in the synthesis gel with HF. For synthesis times less than 3 h, the XRD patterns consist of a broad, featureless signal in the range of 20-25°, characteristic of amorphous silica and with no sign of crystal formation. Similarly, for synthesis times less than 3 h, the Raman spectra show no evidence of D4R formation but do show characteristic bands of the BULKY OSDA. The concurrent absences of D4R signal in the Raman and crystal diffraction peaks in the XRD may indicate that well-defined D4R units can be observed by Raman spectroscopy only when detectable LTA crystals are formed in the synthesis gel.

From 3-6 h of synthesis time, the XRD data in Fig. 4b suggest a transition period of crystal growth. SEM imaging of the 2.5 h sample (Fig. S9a) shows spherical particles with sizes around 400 nm; these particles lack long-range order as shown by XRD (Fig. 4b). SEM of the 3 h sample (Fig. S9b) shows spherical particles in the size range of 400-700 nm; these are partially crystalline by XRD. The final crystal size of the 8 day sample (Fig. S9d) is in the range of 1-2 µm (Fig. S9). The question remains what the Raman spectra in Fig. 4a can reveal about the evolution of D4R units during the formation of the LTA-BULKY-F sample.

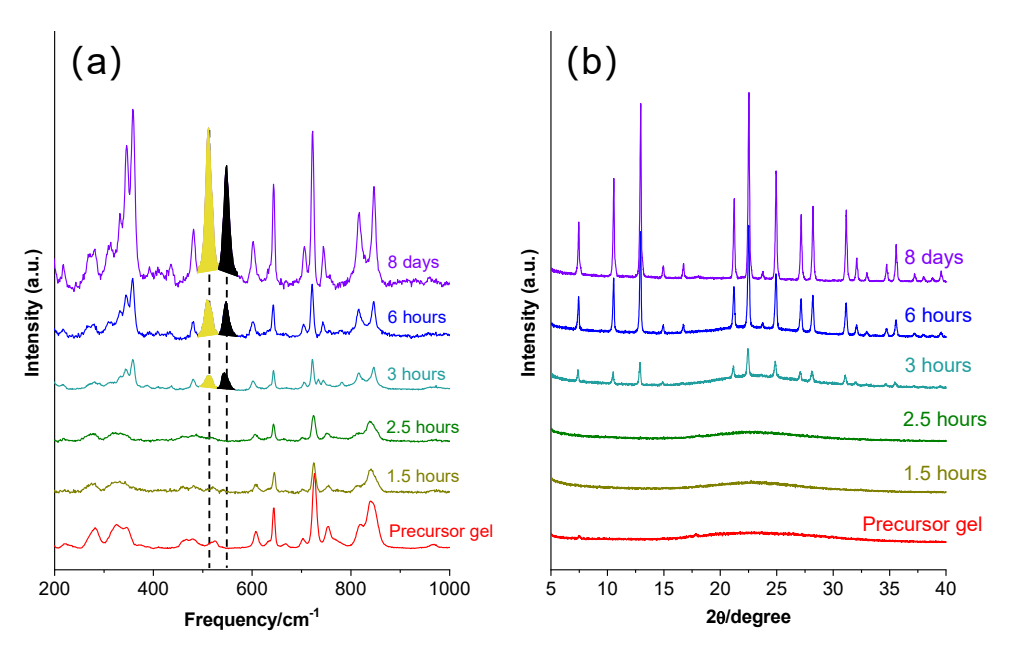


Figure 4. (a) Raman spectra at various stages of LTA synthesis with BULKY, and (b) XRD data for the same samples as (a). LTA crystals appear in XRD at 3 h, as do empty and F-filled D4R bands in Raman spectra.

Focusing now on the 3 h sample, we see the initial emergence of LTA crystals in the XRD data, alongside the early appearance of the empty D4R and F-/D4R bands in the Raman spectra. Although the empty D4R and F-/D4R band locations appear to be constant in time, their relative

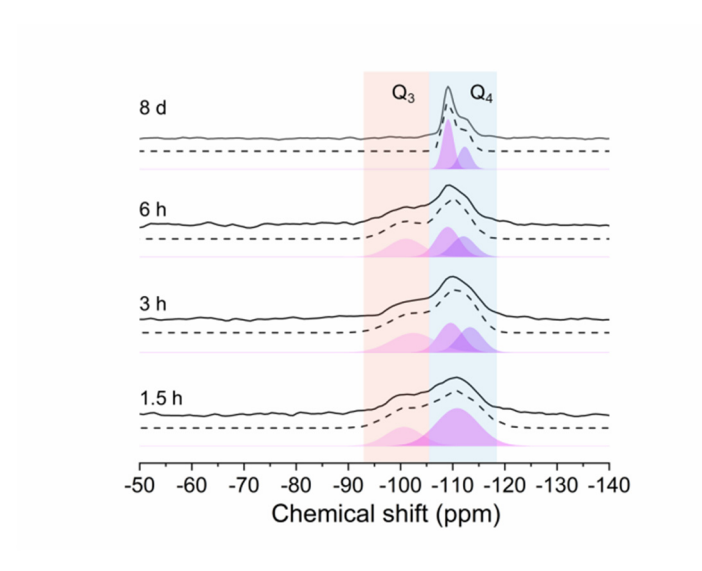


Figure 5. ²⁹Si MAS NMR spectra of LTA-BULKY-F at various stages of LTA synthesis. The 3 h and 6 h samples show the presence of Q_3 Si due to the partial crystallinity of the 2 samples.

intensities (I_F/I_E) are seen to vary with time, with $I_F/I_E = 1.12$ at 3 h and decreasing to 0.75 at 8 day (Table S2). Several hypotheses can potentially explain higher I_F/I_E values at early crystallization times. The first involves possible zones of F^- enrichment in growing LTA crystals, giving more F^- /D4R units than seen at later times. Indeed, we reported above that only 61% of D4R units are F-filled for the fully crystallized sample (8 d); increasing that amount by a factor of 1.12/0.75 (the Raman intensity ratios) would give a possible 91% F-filled D4R. However, there are two problems with this hypothesis. The first involves difficulty with charge balance – additional BULKY cations cannot fit in LTA and there are no other obvious cations in the synthesis mixture to balance charge. The second problem involves F^- ion mobility – once an F^- /D4R unit fully forms the F^- becomes trapped under synthesis temperatures, precluding fluoride redistribution over time. Thus, the F^- enrichment hypothesis fails to explain the Raman data, raising more questions than it answers.

A second possible origin for higher I_F/I_E values at early crystallization times is related to the presence of defects associated with the LTA zeolite structure. As shown in Fig. 5 and Fig. S10, 29 Si NMR spectra of the 1.5 h, 3 h, and 6 h samples show two peaks from Q₃ Si species (i.e., Si atoms with three bridging oxygens and one terminal oxygen) and Q₄ Si species (i.e., Si atoms with four bridging oxygens). The presence of Q₃ and Q₄ Si species in the amorphous 1.5 h sample suggests that the silica species are partially condensed. The Q₃ Si species in the partially crystalline 3 h and 6 h samples are possibly from both amorphous phase and a defect-containing LTA crystalline phase. The Q₃/(Q₄+Q₃) ratios for the 3 h and 6 h samples are 39.2% and 35.1%, respectively, which are similar values. However, the crystallinity of the 6 h sample was found to be much higher than that of the 3 h sample, 80% vs. 33%, which indicates a part of the Q₃ Si species in the partially crystalline 6 h sample must come from Q₃ defects associated with the LTA crystalline phase. With the crystallization time increasing to 8 days, the peak from Q₃ Si species

completely disappears from the ²⁹Si NMR spectrum, suggesting that the defects in the partially crystalline zeolite are healed. Such Q₃ Si species associated with the LTA crystals (6 h sample) can be attributed to either of the following: (*i*) D4R units with a missing Si atom as a point defect, or (*ii*) hydrolyzed Si-O-Si bridges in D4R giving Si-OH/HO-Si defects. Periodic DFT calculations were performed to determine the influence on Raman spectra of placing either a point defect or a hydrolyzed defect into F⁻/D4R and/or empty D4R units (Table S5 and Fig. S12). The calculation results suggest that the presence of hydrolyzed Si-O-Si defects in D4R of LTA-BULKY-F is unlikely because the tightly filled pore space of the as-made zeolite forces the formation of high-energy, pentavalent Si species (Systems 6-10 in Table S5), giving rise to calculated ²⁹Si NMR and Raman spectra (Fig. S12) that look entirely different from those found experimentally. As such, we can rule out hydrolyzed defects causing the varying Raman intensities in Fig. 4a.

Point defects – missing Si atoms with near-neighbor oxygens capped by hydrogens – can be present in both empty D4R and F⁻/D4R. Accordingly, Raman spectra of LTA-BULKY-F with a range of such point defects were calculated (Systems 1-5 in Table S5 and Fig. S12) and compared with experiments. In general, our DFT calculations predict that the presence of point defects in D4R influences both Raman band frequency and intensity. Interestingly, the Raman spectrum for System 1 in Table S5, with one Si point defect in an F⁻/D4R unit, gives the same I_F/I_E ratio seen in experiment for the 3 h sample. However, bands in this calculated Raman spectrum (8F-7F-8E in Fig. S12) exhibit a significant blue shift from those in the defect-free spectrum, an effect that is not seen in experiment.

Alternatively, Fig. 6 shows that averaging computed Raman spectra from the following three systems – (i) the defect-free LTA-BULKY-F system, (ii) LTA-BULKY-F with one point

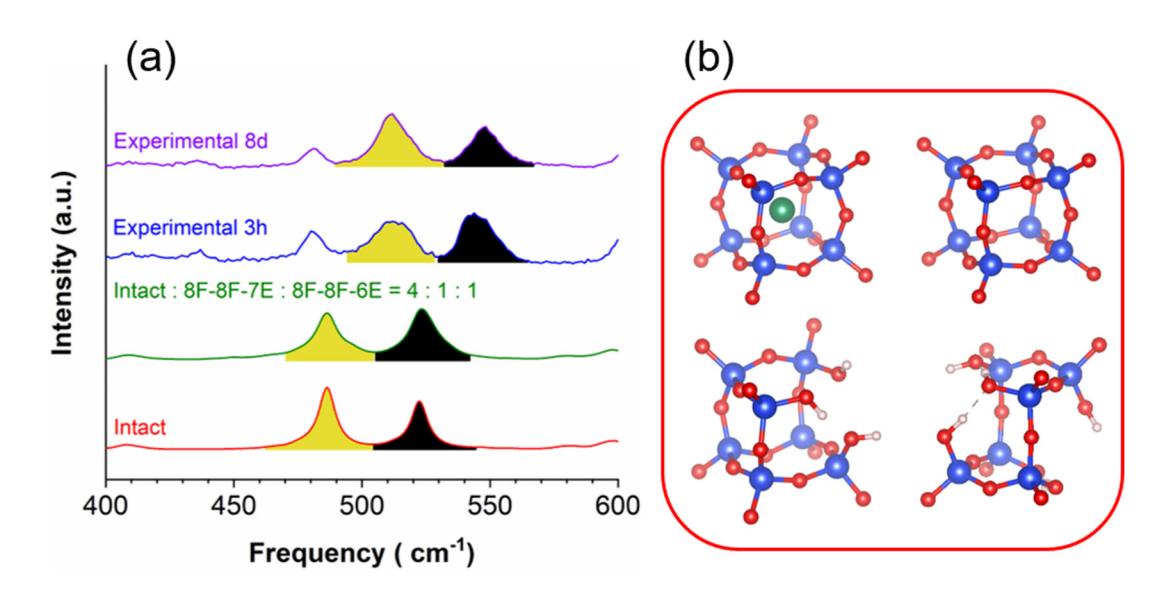


Figure 6. (a) Experimental Raman spectra of fully crystalline LTA-BULKY-F (purple), partially crystalline LTA-BULKY-F (blue), DFT-calculated Raman spectrum of LTA-BULKY-F composed of intact D4Rs (red), and (green) DFT-calculated Raman spectrum combining (i) LTA-BULKY-F only with intact D4Rs, (ii) LTA-BULKY-F with one point defect in an empty D4R in each unit cell, and (iii) LTA-BULKY-F with two point defects in an empty D4R in each unit cell in a 4:1:1 ratio, respectively. (b) (b) Structures of four different D4Rs used for the combined spectrum. From left to right, from top to bottom: intact F-/D4R; intact empty D4R; empty D4R with one missing Si; empty D4R with two missing Si.

defect in an empty D4R in each unit cell (System 2 in Table S5), and (*iii*) LTA-BULKY-F with two point defects in an empty D4R in each unit cell (System 5 in Table S5) – with a ratio of 4:1:1, respectively, reproduces the features of the 3 h experimental sample. In other words, the varying Raman intensities in Fig. 4a indicate the presence and evolution of defects in empty D4R, but not in F⁻/D4R. Peak fitting of the experimental Raman bands at various times gives peak widths (Fig. S11) consistent with this picture, showing that Raman peaks for empty D4R are broader than those for F⁻/D4R, and that the empty D4R bands narrow during crystallization indicating increased ordering. We thus arrive at the conclusion that an important component of zeolite LTA crystal growth involves the healing of point defects in the zeolite framework around otherwise defect-free

F⁻/D4R units, giving strong support for the notion that F⁻ plays a structure-directing role in LTA synthesis.

Synthesis of Siliceous LTA with Reduced Fluoride: Finding new synthesis procedures for making siliceous and high-silica zeolites with much less fluoride is a key target for zeolite chemists because of the expense and challenge of handling HF at industrial scales. The conclusions drawn above – that approximately 2/3 of D4Rs per unit cell in siliceous LTA-BULKY-F are filled with F⁻, and that F⁻ plays a structure-directing role in the formation of D4R – provide key insights that inform a new synthesis of Si-LTA with a substantially reduced amount of F⁻. In the conventional synthesis of LTA-BULKY-F, the molar ratio of F/BULKY is kept close to unity to provide a neutral *p*H environment and sufficient F⁻ to balance OSDA positive charge.

The results of our study suggest that tying the initial HF concentration in the synthesis mixture to the amount of BULKY used in the synthesis may be excessive. In fact, instead of linking the molar composition of F to BULKY, our results suggest linking the molar composition of F to SiO₂ in the ratio HF:SiO₂ = 1:12, based on the target of two F⁻ ions per 24 SiO₂ in the LTA unit cell. We have found that highly crystalline Si-LTA can successfully be obtained with this approach, which reduces the HF/BULKY ratio in the synthesis gel from 1 in the conventional method to 0.17 in the new composition. The amount of F⁻ in the synthesis gel when HF/BULKY is 0.17 equals the value needed to fill 2/3 of the D4Rs in the final LTA crystals, indicating that most of the added F was utilized for D4R formation. We also found that further reducing F⁻ leads to partially crystalline zeolites under these synthesis conditions (Table S6). The Raman spectrum, XRD, and ²⁹Si NMR spectrum of Si-LTA made with this reduced, stoichiometric amount of F⁻ in the initial gel (Fig. S13 and Table S6) are very similar with those from the conventional LTA-BULKY-F

synthesis, indicating that this six-fold reduction of F⁻ in the synthesis can still lead to defect-free highly siliceous LTA zeolites.

CONCLUSIONS

Zeolite synthesis experiments, periodic DFT, Raman spectroscopy, and other characterization methods were applied to investigate the charge-balancing and structure-directing roles of F in zeolite LTA synthesis. Raman spectra show that both empty D4R and F-/D4R can be observed in zeolite LTA synthesized using BULKY as the OSDA in the presence of F. The two different D4Rs show distinct Raman bands due to the geometrical distortion of the D4R and charge transfer to D4R upon inclusion of F. The Raman spectra from the two different D4R units can be used to quantify their distribution in the formed zeolites. Studies on the crystal growth of LTA-BULKY-F suggest that LTA crystals initially emerge with both empty D4R and F-/D4R. We have observed variation in Raman intensities for empty and F-filled D4R during the early stages of LTA crystal growth. Periodic DFT has attributed this variation to the presence of defects in growing LTA crystals, namely, missing Si atoms in empty D4R units. Upon further crystallization these defects appear to become healed, leading to the formation of defect-free LTA zeolite crystals. Our results confirm both the charge-balancing and structure-directing roles of F in zeolite synthesis. These insights were used to reduce the amount of F required to synthesize defect-free, highly siliceous LTA by a factor of 6, which can benefit industrial-scale synthesis of high-silica zeolites.

METHODS

Here we give overviews of experimental and computational methods. Supporting Information Section S2 gives detailed experimental and computational procedures used herein.

Experimental Section

Synthesis of Zeolite (LTA-BULKY-F): 1,2-dimethyl-3-(4-methylbenzyl) imidazolium hydroxide (denoted "BULKY-OH"), was synthesized by following the method previously reported.^{39, 45} Aluminosilicate LTA nanocrystals with a size of around 200 nm were used to as the seeds for the crystallization of siliceous LTA. Such seeds were prepared using a conventional hydrothermal synthesis method in the absence of F⁻ (detailed below and in SI).⁵¹ BULKY was used as an organic structure-directing agent (OSDA) in the synthesis of LTA-BULKY-F by following a method reported previously. 45, 52 Briefly, 10.76 g of aqueous solution of BULKY-OH (0.1872) mmol/g in water) was mixed with 900 µL of tetraethyl orthosilicate (TEOS, 99 wt.%, Alfa Aesar), and the obtained mixture was stirred overnight at room temperature to ensure the hydrolysis of TEOS. Hydrofluoric acid (HF, 48-52 wt.% in water, Alfa Aesar) of 70 μL was then pipetted into the mixture, followed by adding 398 µL of aqueous solution of LTA seeds (42.6 mg/mL; 7 wt.% with regard to the total silica source). Since HF is toxic and especially hazardous to handle, safety procedures should be strictly followed. Water was then evaporated from the suspension at 60 °C, until a final desired composition (1.00 SiO₂: 0.50 HF: 0.50 BULKY: 5.00 H₂O) was achieved. Finally, the crystallization was conducted at 170 °C for 1.5 h, 2.5 h, 3 h, 6 h and 8 days in a 50 mL Teflon-lined stainless-steel autoclave. The synthesized product of about 250 mg was washed by dispersing in DI water of 50 mL and separating using centrifugation. The washing procedure was repeated for 5 times. Part of LTA-BULKY-F samples were calcined under flowing dry air in a tube furnace to remove the BULKY OSDA. The calcination temperature and time were 550 °C and 12 h, respectively, with a ramping rate of 1 °C/min.

Synthesis of LTA seeds: Briefly, first in a 50 mL centrifuge tube, 0.082 mL of NaOH (10 M, Thermo Fisher Scientific) was mixed with 6.65 g of tetramethylammonium hydroxide (TMAOH) (25 wt.% in water, Alfa Aesar) and 3.45 g of deionized (DI) water. Then, silicic acid

(99 wt.%, Sigma Aldrich) of 0.60 g was added. Afterwards, when a transparent solution was achieved under 70 °C and cooled down to RT, 0.50 g aluminum isopropoxide (≥ 98 wt.%, Thermo Fisher Scientific) was added in 2 steps (each with 0.25 g). After getting a complete dissolution of the Al source by employing sonicator and vortex oscillator, the obtained clear solution was transferred into a 50 mL Teflon-lined stainless-steel autoclave for crystallization under 93 °C for 1 day. The obtained LTA seeds were washed through centrifugation using excess DI water until the pH of the supernatant approached neutral. Finally, the LTA seeds were dried under 80 °C in an oven.

Characterizations: The crystalline structure of the zeolite samples was characterized by X-ray diffraction (XRD) using a Rigaku SmartLab diffractometer, which was equipped with Cu-Kα radiation produced at 40 mA and 45 kV, with a step size of 0.016°.

All the LTA samples, including the corresponding precursor gel as well as BULKY-Cl, were characterized using Raman spectroscopy. Raman samples were prepared by dispersing several milligrams of each sample on a gold-coated silicon wafer, and then Raman spectra were recorded by employing an XploRa Raman microscope (Horiba Scientific, USA) operated using a 785 nm laser line as the excitation light source, at ~10 mW power. A 1200-line grating was set, and the laser light was focused on the sample through a 100x magnification lens from Olympus. 20 s scan time and an accumulation of 20 scans were chosen for all the measurements. The laser focus was aimed at the smooth edge part of a particle to ensure favorable light scattering for optimal Raman signal-to-noise ratio. Spectra of multiple particles were obtained to check for consistency. For the BULKY in hydroxide form, its Raman spectrum was obtained in an aqueous solution (0.2 mmol/g). This Raman was performed by employing an EZRaman-I Series High Performance Portable Raman Analyzer (TSI Incorporated, USA) with a 785 nm laser. The

measuring conditions included 170 mW laser power, 2 s averaging parameter, and 5 s integration time.

The structure of BULKY in chloride form was characterized by liquid-state ¹³C NMR on a Bruker 400 MHz NMR spectrometer. Before the measurement, the BULKY in chloride form was dissolved in D₂O.

To test whether fluoride ions were occluded in D4Rs of LTA-BULKY, ¹⁹F MAS SS-NMR spectra were acquired on a Bruker AVANCE 400 wide-bore spectrometer (9.4 T, 376.48 MHz for ¹⁹F), using a 4 mm double resonance probe, operating at a spinning rate of 9.0 kHz. The ¹⁹F direct polarization spectra were collected using the spin-echo sequence with a 2.25 µs of 90° pulse duration for a total of 32 scans. The chemical shift was calibrated using an external reference (sodium fluoride at -121.5 ppm). Data analysis was carried out using with a line broadening factor of 10 Hz.

²⁹Si MAS SS-NMR measurements were performed on a Bruker 600MHz solid-state NMR spectrometer using a 4 mm MAS probe. The spectral operating frequencies were 600.1 and 119.2 MHz for ¹H and ²⁹Si nuclei, respectively, and the samples were spun at 5 kHz during the measurements. A recycle delay time of 100 s was found to be sufficient for the samples.

The amounts of C, H, N and F in the as-made LTA-BULKY sample were measured by Atlantic Microlab at GA, USA, using a flask combustion method followed by ion chromatography. The amounts of Si and Al of the LTA sample after calcination were measured at Galbraith Laboratories at TN, USA, using inductively coupled plasma atomic emission spectroscopy (ICP-OES). The samples were dried at 120 °C for 12 hours before measurements to remove adsorbed water.

Thermogravimetric analysis (TGA) was conducted on a thermogravimetric analyzer (SDT600, TA). For each measurement, about 10 mg of the sample was used. The temperature was programmed from RT to 900 °C (with a ramping rate of 1 °C/min), and finally held for 2 h with an air flow of 10 mL/min.

Scanning electron microscope (SEM) was utilized to determine the morphology of the LTA-BULKY-F samples at different crystallization times. The SEM images were collected using a FEI Magellan 400 XHR-SEM instrument, which is equipped with a field-emission gun operated at 3.0 kV. Prior to this characterization, all the samples were sputter coated with platinum for a better imaging quality.

Computational Section

Zeolite LTA systems containing BULKY and fluoride ions (F⁻) were studied using periodic density functional theory (DFT) via planewave basis sets with the Vienna Ab initio Simulation Package (VASP).⁵³ The structure of zeolite LTA was adopted from our previous work.³⁹ For all DFT periodic simulations reported here, we applied the projector augmented wave (PAW)⁵⁴⁻⁵⁵ pseudo-potential and the Perdew-Burke-Ernzerhof (PBE)⁵⁶ exchange-correlation functional with the D3 dispersion corrections⁵⁷⁻⁵⁸ and non-spherical corrections, using an energy cutoff value of 480 eV, a 1×1×1 K-point mesh and Gaussian smearing of which the width is 0.05 eV. Avogadro⁵⁹ was used to initially combine the LTA framework with BULKY and F so that 2 BULKY cations are inside the α-cage and 2 fluoride ions are inside D4Rs. *Ab initio* molecular dynamics (AIMD) simulations with NVT ensemble (Nose-Hoover thermostat)⁶⁰⁻⁶¹ were then performed for 1 ps to identify stable configurations of the LTA-BULKY-F systems at 443 K, which is the experimental synthesis temperature of LTA-BULKY-F.⁴⁵ Such systems were optimized from initial conditions extracted at random from AIMD, to identify minimum-energy configurations for normal mode

analysis (NMA) until the energy of ionic steps varied within 10⁻⁴ eV. The optimizations also relaxed unit cell lattice parameters. Initial structures of defected systems were made based on the optimized intact LTA-BULKY-F system. For Si-missing defects (point defects), selected Si atoms were deleted, and their surrounding O atoms were compensated by H atoms to form –OH terminals. For hydrolyzed defects, a water molecule was added across an Si-O-Si tricyclic bridge leading to two OH terminal defects.³⁹ NMA was performed to determine vibrational frequencies and normal mode vibrational coordinates. Density functional perturbation theory (DFPT) was used to compute intensities of Raman bands in the frequency ranges of interest. To better mimic experimental Raman spectra, Lorentzian-line broadening was applied to calculated spectral lines using a full band width at half maximum (FWHM) of 5 cm⁻¹. Visualizations of optimized structures and normal modes were performed on VESTA.⁶²

ASSOCIATED CONTENT

Supporting Information. Raman Spectra of OSDA in solid and solution; DFT-computed structural properties; Comparison of Raman intensity ratios; Collective D4R normal modes and symmetries; Raman band shape analysis; TGA of as-made LTA; DFT-computed NMR chemical shifts; Elemental analysis of as-made LTA; Experimental ¹⁹F MAS SS-NMR of as-made LTA with recycle delay time analysis; XRD of LTA seeds with and without HF; SEM of as-made LTA vs. time; ²⁹Si MAS SS-NMR of as-made LTA with deconvolution analysis vs. time; DFT-computed Raman spectra of various defect models; Raman, XRD, and ²⁹Si MAS SS-NMR of as-made LTA with minimal HF; Detailed Experimental and Computational Methods; Coordinates for all important DFT calculations. This material is available free of charge via the Internet at http://pubs.acs.org.

AUTHOR INFORMATION

*Corresponding Author Emails: auerbach@umass.edu, wfan@ecs.umass.edu

Author Contributions

*S.L. and T.W. contributed equally to this work.

S.L. designed and carried out all syntheses, performed characterizations including some Raman,

and organized the experimental data for publication; T.K. designed and carried out all calculations,

performed intensity analyses on all Raman spectra, and organized computational data for

publication; L.Q. designed and carried out all the F NMR measurements; J.K. carried out all the

Si NMR measurements; G.T. designed and carried out most of the Raman measurements; M.T.,

S.M.A., and W.F. coordinated the project and wrote the paper.

ACKNOWLEDGMENTS

S.M.A. and W.F. gratefully acknowledge support from the U.S. Department of Energy, Office of

Science, Basic Energy Sciences, Materials Sciences and Engineering Division, under Award #

DE-SC0019170. We thank the Massachusetts Green High-Performance Computing Center for

generous access to computing facilities, and we thank Dr. Woody Sherman and Silicon

Therapeutics for further access to computational resources. W.F. gratefully acknowledges National

Science Foundation Major Research Instrumentation Program (CHE-1726578) for supporting the

powder X-ray diffractometer, and Sanket Sabnis for the SEM measurement. L.Q. is supported by

the U.S. Department of Energy (DOE), Office of Basic Energy Sciences, Division of Chemical

Sciences, Geosciences, and Biosciences. The Ames Laboratory is operated for the U.S. DOE by

Iowa State University under Contract No. DE-AC02-07CH11358.

27

REFERENCES

- 1. Davis, M. E., Ordered porous materials for emerging applications. *Nature* **2002**, *417* (6891), 813-821.
- 2. Davis, M. E., Zeolites from a materials chemistry perspective. *Chem. Mater.* **2013**, 26 (1), 239-245.
- 3. Corma, A., From microporous to mesoporous molecular sieve materials and their use in catalysis. *Chem. Rev.* **1997**, *97* (6), 2373-2419.
- 4. Auerbach, S. M.; Karrado, K. A.; Dutta, P. K., *Handbook of Zeolite Science and Technology*. Marcel Dekker: New York, 2003; p 1184.
- 5. Cundy, C. S.; Cox, P. A., The hydrothermal synthesis of zeolites: History and development from the earliest days to the present time. *Chem. Rev.* **2003**, *103* (3), 663-701.
- 6. Davis, M. E.; Lobo, R. F., Zeolite and molecular sieve synthesis. *Chem. Mater.* **1992**, *4* (4), 756-768.
- 7. Jiang, J. X.; Yu, J. H.; Corma, A., Extra-large-pore zeolites: bridging the gap between micro and mesoporous structures. *Angew. Chem.-Int. Edit.* **2010**, *49* (18), 3120-3145.
- 8. Mintova, S.; Olson, N. H.; Valtchev, V.; Bein, T., Mechanism of zeolite a nanocrystal growth from colloids at room temperature. *Science* **1999**, *283* (5404), 958-960.
- 9. Davis, T. M.; Drews, T. O.; Ramanan, H.; He, C.; Dong, J. S.; Schnablegger, H.; Katsoulakis, M. A.; Kokkoli, E.; McCormick, A. V.; Penn, R. L.; Tsapatsis, M., Mechanistic principles of nanoparticle evolution to zeolite crystals. *Nat. Mater.* **2006**, *5* (5), 400-408.
- 10. Lupulescu, A. I.; Rimer, J. D., In Situ imaging of silicalite-1 surface growth reveals the mechanism of crystallization. *Science* **2014**, *344* (6185), 729-732.
- 11. Earl, D. J.; Deem, M. W., Toward a database of hypothetical zeolite structures. *Ind. Eng. Chem. Res.* **2006**, *45* (16), 5449-5454.
- 12. Foster, M. D.; Treacy, M. M. J. A Database of hypothetical zeolite structures: http://www.hypotheticalzeolites.net (accessed 2020-09-14).
- 13. Li, Y.; Yu, J., New stories of zeolite structures: their descriptions, determinations, predictions, and evaluations. *Chem. Rev.* **2014**, *114* (14), 7268-7316.
- 14. Lin, L. C.; Berger, A. H.; Martin, R. L.; Kim, J.; Swisher, J. A.; Jariwala, K.; Rycroft, C. H.; Bhown, A. S.; Deem, M.; Haranczyk, M.; Smit, B., In silico screening of carbon-capture materials. *Nat. Mater.* **2012**, *11* (7), 633-641.
- 15. Bai, P.; Jeon, M. Y.; Ren, L.; Knight, C.; Deem, M. W.; Tsapatsis, M.; Siepmann, J. I., Discovery of optimal zeolites for challenging separations and chemical transformations using predictive materials modeling. *Nat. Commun.* **2015**, *6* (1), 5912.
- 16. Barrer, R. M., Hydrothermal Chemistry of Zeolites. Academic Press: London, 1982.
- 17. Camblor, M. A.; Villaescusa, L. A.; Díaz-Cabañas, M. J., Synthesis of all-silica and high-silica molecular sieves in fluoride media. *Top. Catal.* **1999**, *9* (1), 59-76.
- 18. Flanigen, E. M.; Patton, R. L. Polymorph and process for preparing same. U.S. Patent 4,073,865,, 1978.

- 19. Caullet, P.; Paillaud, J.-L.; Simon-Masseron, A.; Soulard, M.; Patarin, J., The fluoride route: a strategy to crystalline porous materials. *C. R. Chim.* **2005**, *8* (3), 245-266.
- 20. Goesten, M. G.; Hoffmann, R.; Bickelhaupt, F. M.; Hensen, E. J. M., Eight-coordinate fluoride in a silicate double-four-ring. *Proc. Natl. Acad. Sci. U. S. A.* **2017**, *114* (5), 828-833.
- 21. Villaescusa, L. A.; Wheatley, P. S.; Bull, I.; Lightfoot, P.; Morris, R. E., The location and ordering of fluoride ions in pure silica zeolites with framework types IFR and STF; implications for the mechanism of zeolite synthesis in fluoride media. *J. Am. Chem. Soc.* **2001**, *123* (36), 8797-8805.
- 22. Villaescusa, L. A.; Bull, I.; Wheatley, P. S.; Lightfoot, P.; Morris, R. E., The location of fluoride and organic guests in 'as-made' pure silica zeolites FER and CHA. *J. Mater. Chem.* **2003**, *13* (8), 1978-1982.
- 23. Shayib, R. M.; George, N. C.; Seshadri, R.; Burton, A. W.; Zones, S. I.; Chmelka, B. F., Structure-directing roles and interactions of fluoride and organocations with siliceous zeolite frameworks. *J. Am. Chem. Soc.* **2011**, *133* (46), 18728-18741.
- 24. Barrett, P. A.; Camblor, M. A.; Corma, A.; Jones, R. H.; Villaescusa, L. A., Synthesis and structure of as-prepared ITQ-4, a large pore pure silica zeolite: the role and location of fluoride anions and organic cations. *J. Phys. Chem. B* **1998**, *102* (21), 4147-4155.
- 25. Axon, S. A.; Klinowski, J., Synthesis and characterization of defect-free crystals of MFI-type zeolites. *Appl. Catal. A-Gen.* **1992**, *81* (1), 27-34.
- 26. Zicovich-Wilson, C. M.; Gándara, F.; Monge, A.; Camblor, M. A., In Situ transformation of TON silica zeolite into the less dense ITW: structure-direction overcoming framework instability in the synthesis of SiO2 zeolites. *J. Am. Chem. Soc.* **2010**, *132* (10), 3461-3471.
- 27. Corma, A.; Puche, M.; Rey, F.; Sankar, G.; Teat, S. J., A zeolite structure (ITQ-13) with three sets of medium-pore crossing channels formed by 9- and 10-rings. *Angew. Chem.-Int. Edit.* **2003**, *42* (10), 1156-1159.
- 28. Villaescusa, L. A.; Barrett, P. A.; Camblor, M. A., ITQ-7: A new pure silica polymorph with a three-dimensional system of large pore channels. *Angew. Chem.-Int. Edit.* **1999**, *38* (13 14), 1997-2000.
- 29. Corma, A.; Rey, F.; Rius, J.; Sabater, M. J.; Valencia, S., Supramolecular self-assembled molecules as organic directing agent for synthesis of zeolites. *Nature* **2004**, *431* (7006), 287-290.
- 30. Zhou, Y.; Kadam, S. A.; Shamzhy, M.; Čejka, J.; Opanasenko, M., Isoreticular UTL-derived zeolites as model materials for probing pore size activity relationship. *ACS Catal.* **2019**, *9* (6), 5136-5146.
- 31. Roth, W. J.; Nachtigall, P.; Morris, R. E.; Wheatley, P. S.; Seymour, V. R.; Ashbrook, S. E.; Chlubná, P.; Grajciar, L.; Položij, M.; Zukal, A.; Shvets, O.; Čejka, J., A family of zeolites with controlled pore size prepared using a top-down method. *Nat. Chem.* **2013**, *5* (7), 628-633.
- 32. Mazur, M.; Wheatley, P. S.; Navarro, M.; Roth, W. J.; Položij, M.; Mayoral, A.; Eliášová, P.; Nachtigall, P.; Čejka, J.; Morris, R. E., Synthesis of 'unfeasible' zeolites. *Nat. Chem.* **2016**, *8* (1), 58-62.
- 33. George, A. R.; Catlow, C. R. A., A computational study of the role of F⁻ ions in the octadecasil structure. *Zeolites* **1997**, *18* (1), 67-70.

- 34. Liu, X.; Ravon, U.; Tuel, A., Fluoride removal from double four-membered ring (D4R) units in as-synthesized Ge-containing zeolites. *Chem. Mater.* **2011**, *23* (22), 5052-5057.
- 35. Database of zeolite structure, http://www.iza-structure.org/databases (accessed 2020-09-14)
- 36. Zhang, G.; Wang, B.; Zhang, W.; Li, M.; Tian, Z., Synthesis of polymorph A-enriched beta zeolites in a HF-concentrated system. *Dalton Trans.* **2016**, *45* (15), 6634-6640.
- 37. Dutta, P. K.; Rao, K. M.; Park, J. Y., Correlation of raman spectra of zeolites with framework architecture. *J. Phys. Chem.* **1991**, *95* (17), 6654-6656.
- 38. Geisler, T.; Dohmen, L.; Lenting, C.; Fritzsche, M. B. K., Real-time in situ observations of reaction and transport phenomena during silicate glass corrosion by fluid-cell Raman spectroscopy. *Nat. Mater.* **2019**, *18* (4), 342-348.
- 39. Wang, T.; Luo, S.; Tompsett, G. A.; Timko, M. T.; Fan, W.; Auerbach, S. M., Critical role of tricyclic bridges including neighboring rings for understanding raman spectra of zeolites. *J. Am. Chem. Soc.* **2019**, *141* (51), 20318-20324.
- 40. Fan, F.; Feng, Z.; Li, C., UV raman spectroscopic studies on active sites and synthesis mechanisms of transition metal-containing microporous and mesoporous materials. *Acc. Chem. Res.* **2010**, *43* (3), 378-387.
- 41. Yu, Y.; Xiong, G.; Li, C.; Xiao, F. S., Characterization of aluminosilicate zeolites by UV Raman spectroscopy. *Microporous Mesoporous Mater.* **2001**, *46* (1), 23-34.
- 42. Cundy, C. S.; Cox, P. A., The hydrothermal synthesis of zeolites: precursors, intermediates and reaction mechanism. *Microporous Mesoporous Mater.* **2005**, *82* (1–2), 1-78.
- 43. Wakihara, T.; Suzuki, Y.; Fan, W.; Saito, S.; Kohara, S.; Sankar, G.; Sanchez-Sanchez, M.; Ogura, M.; Okubo, T., Changes in the medium-range order during crystallization of aluminosilicate zeolites characterized by high-energy X-ray diffraction technique. *J. Ceram. Soc. Japan* **2009**, *117* (1363), 277-282.
- 44. Suzuki, Y.; Wakihara, T.; Kohara, S.; Itabashi, K.; Ogura, M.; Okubo, T., Mechanistic study on the synthesis of a porous zincosilicate VPI-7 containing three-membered rings. *J. Phys. Chem. C.* **2011**, *115* (2), 443-446.
- 45. Boal, B. W.; Schmidt, J. E.; Deimund, M. A.; Deem, M. W.; Henling, L. M.; Brand, S. K.; Zones, S. I.; Davis, M. E., Facile synthesis and catalysis of pure-silica and heteroatom LTA. *Chem. Mater.* **2015**, *27* (22), 7774-7779.
- 46. Dutta, P. K.; Del Barco, B., Raman spectroscopy of zeolite A: influence of silicon/aluminum ratio. *J. Phys. Chem.* **1988**, *92* (2), 354-357.
- 47. Villaescusa, L. A.; Márquez, F. M.; Zicovich-Wilson, C. M.; Camblor, M. A., Infrared investigation of fluoride occluded in double four-member rings in zeolites. *J. Phys. Chem. B.* **2002**, *106* (10), 2796-2800.
- 48. George, A. R.; Catlow, C. R. A., An investigation into the effects of ion incorporation on the electronic structure of silicate fragments via ab initio computational techniques. *Chem. Phys. Lett.* **1995**, *247* (4-6), 408-417.
- 49. Helfrecht, B. A.; Semino, R.; Pireddu, G.; Auerbach, S. M.; Ceriotti, M., A new kind of atlas of zeolite building blocks. *J. Chem. Phys.* **2019**, *151* (15), 154112.

- 50. Ogura, M.; Kawazu, Y.; Takahashi, H.; Okubo, T., Aluminosilicate species in the hydrogel phase formed during the aging process for the crystallization of FAU zeolite. *Chem. Mater.* **2003**, *15* (13), 2661-2667.
- 51. Fan, W.; Shirato, S.; Gao, F.; Ogura, M.; Okubo, T., Phase selection of FAU and LTA zeolites by controlling synthesis parameters. *Microporous Mesoporous Mater.* **2006**, 89 (1), 227-234.
- 52. Jo, D.; Ryu, T.; Park, G. T.; Kim, P. S.; Kim, C. H.; Nam, I.-S.; Hong, S. B., Synthesis of high-silica LTA and UFI zeolites and NH₃–SCR performance of their copper-exchanged form. *ACS Catal.* **2016**, *6* (4), 2443-2447.
- 53. Kresse, G.; Furthmüller, J., Efficient iterative schemes for ab initio total-energy calculations using a plane-wave basis set. *Phys. Rev. B Condens. Matter.* **1996,** *54* (16), 11169-11186.
- 54. Kresse, G.; Joubert, D., From ultrasoft pseudopotentials to the projector augmented-wave method. *Phys. Rev. B Condens. Matter.* **1999**, *59* (3), 1758-1775.
- 55. Blöchl, P. E., Projector augmented-wave method. *Phys. Rev. B Condens. Matter.* **1994**, *50* (24), 17953-17979.
- 56. Perdew, J. P.; Burke, K.; Ernzerhof, M., Generalized gradient approximation made simple. *Phys. Rev. Lett.* **1996**, *77* (18), 3865-3868.
- 57. Grimme, S.; Antony, J.; Ehrlich, S.; Krieg, H., A consistent and accurate ab initio parametrization of density functional dispersion correction (DFT-D) for the 94 elements H-Pu. *J. Chem. Phys.* **2010**, *132* (15), 154104.
- 58. Grimme, S.; Ehrlich, S.; Goerigk, L., Effect of the damping function in dispersion corrected density functional theory. *J. Comput. Chem.* **2011**, *32* (7), 1456-1465.
- 59. Hanwell, M. D.; Curtis, D. E.; Lonie, D. C.; Vandermeersch, T.; Zurek, E.; Hutchison, G. R., Avogadro: an advanced semantic chemical editor, visualization, and analysis platform. *J. Cheminformatics* **2012**, *4* (1), 17.
- 60. Nosé, S., A unified formulation of the constant temperature molecular dynamics methods. *J. Chem. Phys.* **1984**, *81* (1), 511-519.
- 61. Frenkel, D.; Smit, B., *Understanding molecular simulation: from algorithms to applications*. Elsevier: 2001; Vol. 1.
- 62. Momma, K.; Izumi, F., VESTA 3 for three-dimensional visualization of crystal, volumetric and morphology data. *J. Appl. Crystallogr.* **2011**, *44* (6), 1272-1276.

